Materials Synthesis and Processing Using Ion Beams, R.J. Culbertson, O.W. Holland, K.S. Jones, and K Maex, eds. (Mat. Res. Soc. Proc., Pittsburgh, PA, 1994), pp. 197-204.

Modeling of Dopant Diffusion during Annealing of Sub-Amorphizing Implants

SCOTT DUNHAM, Electrical, Computer and Systems Engineering Department, Boston University, Boston, MA 02215

Introduction

Ion implant annealing is a complicated process involving the interactions of point defects generated during the implantation, implanted or previously present dopants, and extended defects which form as a result of the implant damage. To effectively model the process, it is essential to determine the critical processes, assess the validity of assumptions and calculate appropriate parameter values. In addition, implant annealing is just one element in the VLSI fabrication process, and the model development must consider the process as part of the broad range of experimental observations, as it is only through consistent physical models that simulators can predict the multiple interactions and two and three-dimensional effects present in VLSI structures. This work focuses on enhanced diffusion following silicon implants below the amorphization threshold as a function of dose, energy and time.

Initial Defect/Damage Profiles

Enhanced diffusion during implant annealing is due to the damage generated by the implantation process. For subamorphizing implants, the damage can be considered as existing of point defects or small aggregates of point defects (e.g., divacancies). In this work, we use defect profiles generated using TRIM-CSR [1, 2], a Monte-Carlo simulator which includes the full collision cascade, sputtering of atoms near the surface, and replacement reactions. Due to the collision cascade, the resulting defect distribution is much larger ($\sim$ 1000 times) than the implant profile, with vacancy and interstitial distributions which are nearly identical. The interstitial distribution is slightly displaced towards bulk, making the surface vacancy-rich and the bulk interstitial-rich. As an example, Figure 1 shows simulated defect distribution in the substrate for a 80 keV silicon implant.

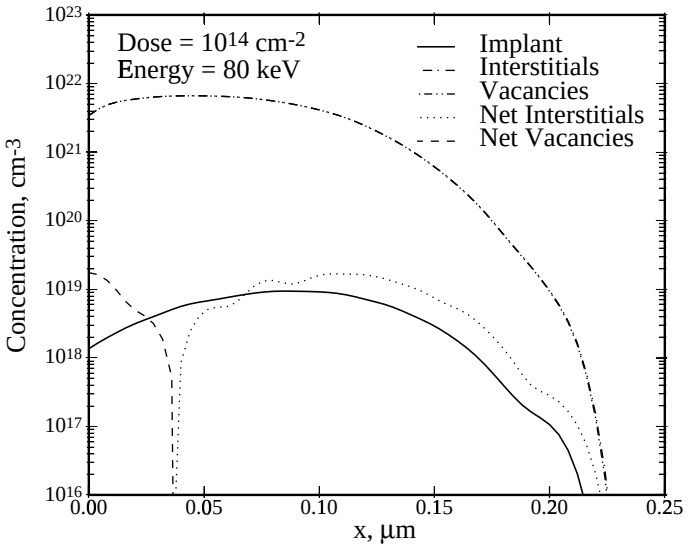

Figure 1: *Total and net defect concentrations simulated with TRIMCSR for a* $10^{14}\mathrm{cm}^{-2}$ *80 keV silicon implant into a silicon wafer with a 30 nm cap oxide. The knock-on oxygen is not included in the interstitial density, since it is not substitutional.*

Ideally, the net silicon excess would just equal the implant dose — the number of excess atoms. However, this does not account for sputtering, which reduces net excess at low energies for uncapped silicon, or capping layers, which result in knock-ons and can end up containing much or all of the vacancy-rich region. In addition, the interstitial-rich layer extends significantly below implant due to the collision cascade. Figure 2 illustrates the

difference in damage profiles between capped and uncapped implants. Any surface regrowth during the implant itself is ignored; however, defects shallow enough to reach the surface during the implant would regrow rapidly during the subsequent annealing simulation. It is clear that assuming the net defect profile (interstitial minus vacancy) is just equal to the implant profile (sometimes called the +1 Model [3]) does not account for changes in energy and capping layer, particularly for low energies (shallow junctions). For bare silicon, sputtering results in a loss of excess material at low energies resulting in the net defect dose being less than the implant dose. In contrast, for implantation through the cap oxide, the net defect dose exceeds the implant dose in the substrate at low energies since much of the vacancy-rich region is in the capping layer. The effect of a capping layer is very dependent on the film composition. For implantation through a film whose components are all primarily substitutional in silicon, the net defect dose is much greater than the implant dose, while for a film whose components are all primarily interstitial, the resulting net defect dose will be similar to bare silicon. The example considered here — an oxide capping layer — falls in between these two extremes.

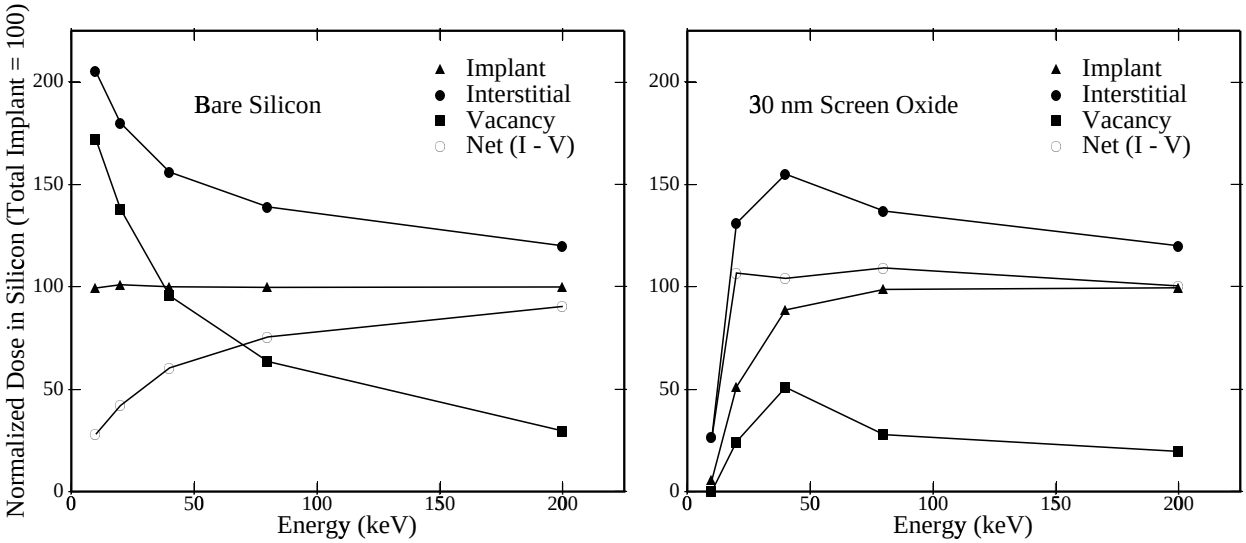

Figure 2: *Simulated net defect and implant doses in substrate* (cm^{-2}) *versus implant energy for* $10^{14}\mathrm{cm}^{-3}$ *silicon implants into (a) bare silicon and (b) silicon with 30 nm cap oxide. Doses are determined by integrating concentration profiles over depth.*

Experimental Sources

In this work, we will focus on modeling of annealing of silicon self-implantation for doses below the amorphization threshold. The experimental data is primarily from Packan [4], with additional data from Park and Law [5] and Cowern [6]. In all cases, the diffusion of a low-dose dopant marker layer which was fully annealed prior to the silicon implant was used to monitor the defect concentrations. This system is particularly appropriate for testing models because the implant energy and dose can be varied independently without altering the initial marker layer or Fermi level.

Some of the observations that have been made from such experiments are that enhanced diffusion increases with increased energy, but has only a relatively weak dependence on dose. In addition, when the time-dependent behavior is observed, it has been found that there is an effective peak diffusivity enhancement. That is, higher doses or energies gives longer transient, but not higher peak diffusivity. Also, interstitial clusters have been observed following short anneals, but disappear after longer anneals [6].

Models

Absolute defect profiles are very sensitive to implant simulation parameters such as the threshold energy for generating Frenkel pairs. However, the enhanced diffusion during annealing depends primarily on net defect profiles, that is the difference between the interstitial and vacancy profiles, which are much less dependent on implant models. This is because the high initial defect concentrations result in very fast recombination and thus the initial decay to the net defect concentration is so fast that the enhanced diffusion during that period can be neglected. To illustrate this, consider approximately equal defect concentrations much greater than the equilibrium values. The defect concentration is then given by

$$C_{\mathrm{I}} \cong C_{\mathrm{V}} \cong \frac{C(0)}{1 + k_r C(0) t}. \tag{1}$$

If the dopant diffusivity remains proportional to the defect concentrations even for the extremely high supersaturations present during implant annealing conditions, the amount of diffusion during the time (τ_1) required to reduce the initial profiles to the net profiles is

$$(Dt)_{\mathrm{excess}} \cong \frac{D^*}{k_r} \left(\frac{f_{\mathrm{I}}}{C_{\mathrm{I}}^*} + \frac{1 - f_{\mathrm{I}}}{C_{\mathrm{V}}^*} \right) \ln \frac{C(0)}{C^{\mathrm{net}}}, \tag{2}$$

which is small compared to observed profile motions. For diffusivity limited to some peak value as observed experimentally, the effect is even smaller and is given by the peak diffusivity times τ_1. The length of the initial transient period is approximately

$$\tau_1 \cong \frac{1}{k_r C^{\mathrm{net}}} \sim 0.2\mathrm{sec} \text{ at } 800^{\circ}\mathrm{C}, \tag{3}$$

which is negligible compared to the period over which transient enhanced diffusion persists [4]. Therefore, there is very little loss in accuracy by starting with net defect profiles (added to equilibrium values), which results in much faster simulations. Comparing simulations starting with total and net initial defect profiles bears this out as the resulting profile motion differs by less than 0.2%.

As mentioned above, experiments which have examined the time dependence of enhanced diffusion due to ion implantation have consistently observed an upper limit on diffusivity enhancement independent of implant dose or energy [4, 6]. There are two effects which are likely to limit dopant diffusivity in the presence of large defect supersaturations: dopant/defect pairing [14] and interstitial cluster formation [6]. Both are known to occur, the question is which limits maximum diffusivity.

Dopant diffusion occurs via dopant/defect pairs. Under normal circumstances, paired dopants are a small fraction of total and $C_{\mathrm{AX}} = K_{\mathrm{AX}} C_{\mathrm{A}} C_{\mathrm{X}}$. For large defect supersaturation (as during implant annealing) the number of pairs is limited by the number of dopants:

$$C_{\mathrm{AX}} = \frac{K_{\mathrm{AX}} C_{\mathrm{A}} C_{\mathrm{X}}}{1 + K_{\mathrm{AX}} C_{\mathrm{X}}}. \tag{4}$$

Interstitial clusters have been observed following sub-amorphizing anneals and these clusters disappear during subsequent annealing [6]. As a simple model of the effects of interstitial aggregation, we can consider an effective solid solubility of interstitials which limits the peak free interstitial density:

$$C_{\mathrm{I}}^{\mathrm{free}} = \min(C_{\mathrm{I}}^{\mathrm{total}}, C_{\mathrm{I}}^{\mathrm{ss}}). \tag{5}$$

Qualitatively, both effects give the observed time dependence of enhanced diffusion. However, the two models predict very different transient period lengths, dose dependences and energy dependences.

Parameter	Value	Reference
$D_{\rm I}C_{\rm I}^*$	$9.0 \times 10^2\,{\rm cm}^{-1}{\rm sec}^{-1}$	[7]
$D_{\rm V}C_{\rm V}^*$	$5.1 \times 10^3\,{\rm cm}^{-1}{\rm sec}^{-1}$	[8]
$D_{\rm I}$	$2.1 \times 10^{-9}\,{\rm cm}^2/{\rm sec}$	[9]
$C_{\rm V}^*$	$1.0 \times 10^{13}\,{\rm cm}^{-3}$	[7]
k_r	$3.2 \times 10^{-15}{\rm cm}^3/{\rm sec}$	[10]
$D_{\rm B}^*$	$3.3 \times 10^{-17}\,{\rm cm}^2/{\rm sec}$	[4]

Table I: *Parameter values at 800°C used in modeling.*

Comparison to Experiments

The simulations were performed using the dial-an-operator feature of the simulation software PEPPER [11]. Either pairing or interstitial clustering was included to limit the peak diffusivity, with fitting parameters interstitial interface recombination velocity ($\sigma_{\rm I}$) and the factor limiting peak diffusion enhancement ($C_{\rm I}{}^{ss}/C_{\rm I}^*$ or $1/K_{\rm AI}C_{\rm I}^*$) determined using the Levenberg-Marquardt optimizer PROFILE [12]. All other parameters were as determined from previously published work as summarized in Table I. Many of these parameters are noncritical because the simulation results are nearly independent of vacancy interactions ($D_{\rm V}$, $C_{\rm V}^*$, $\sigma_{\rm V}$, k_r) since very quickly $C_{\rm I} \gg C_{\rm I}^*$ and $C_{\rm V} \ll C_{\rm V}^*$ due to interstitial diffusion and recombination.

Figures 3, 4 and 5 show the comparison between the pairing model and data from Packan [4], while Figures 5, 6 and 7 show the comparison to the clustering model. In both cases, a single set of parameters are used for all the simulations.

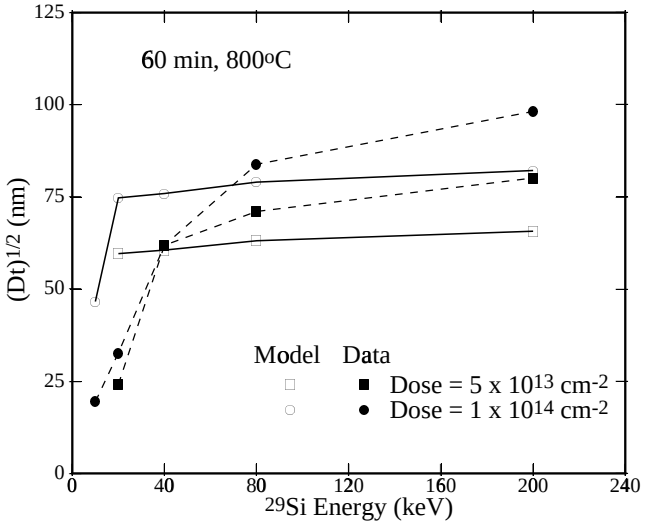

Figure 3: *Simulated profile movements for the pairing model versus implant energy for two different implant doses compared to experimental data from Packan [4].*

Discussion

For both models, the final excess Dt is determined by the product of peak diffusivity ($f_{\rm I}D^*/K_{\rm AX}C_{\rm I}^*$ or $f_{\rm I}D^*C_{\rm I}{}^{ss}/C_{\rm I}^*$) and the length of the transient period. For the pairing model, because interstitial diffusivity is high and all interstitials are free to diffuse, the length of transient is primarily determined by the interface regrowth velocity $\sigma_{\rm I}$.

Figure 8 shows a series of simulated defect profiles for the pairing model. Note that the excess interstitial profile extends to substantial depths into the substrate. We can estimate the time evolution of $Q_{\rm I}$, the net excess interstitial dose by

$$\frac{dQ_{\rm I}}{dt} \sim -\frac{\sigma_{\rm I}Q_{\rm I}}{\sqrt{D_{\rm I}t + (\Delta R_p)^2}} \tag{6}$$

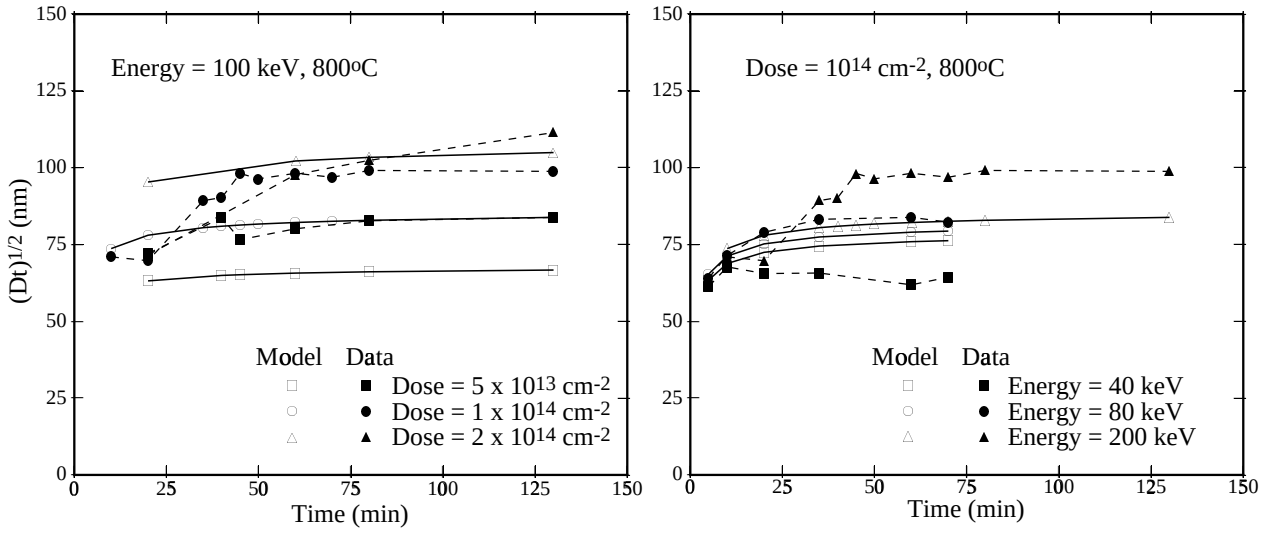

Figure 4: *Simulated profile movements for the pairing model versus annealing time as a function of (a) implant dose and (b) implant energy compared to experimental data from Packan [4].*

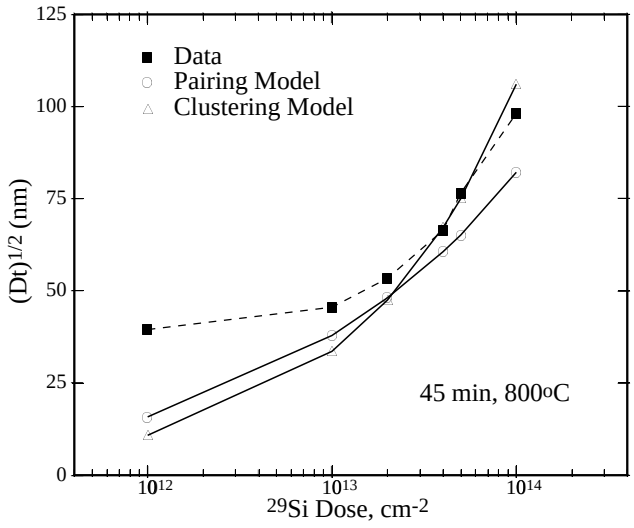

Figure 5: *Simulated profile movements versus implant dose for both models compared to experimental data from Packan [4].*

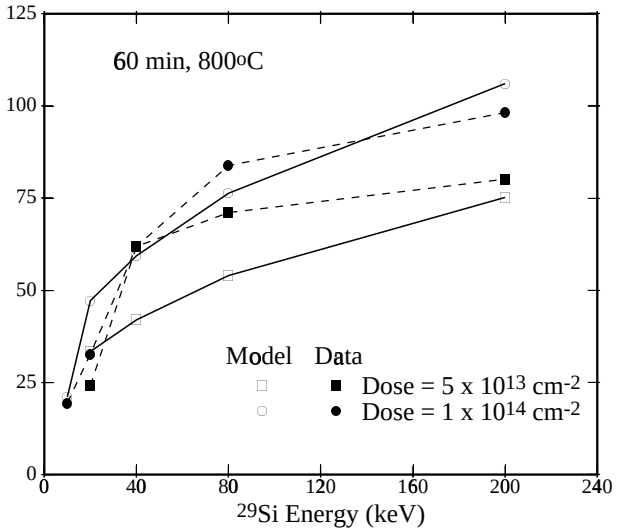

Figure 6: *Simulated profile movements for the pairing model versus implant energy for two different implant doses compared to experimental data from Packan [4].*

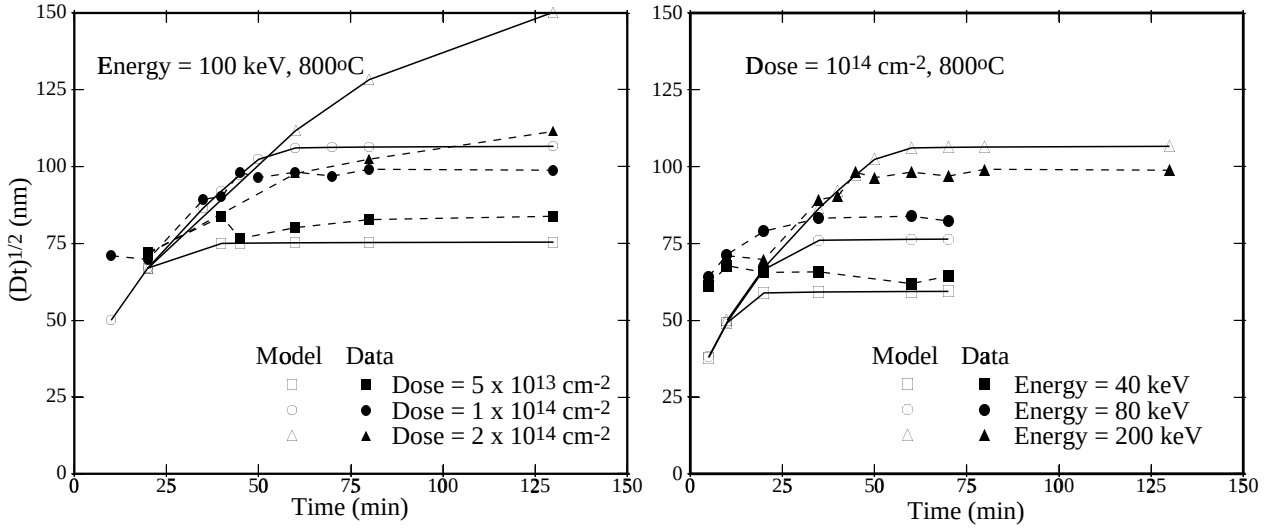

Figure 7: *Simulated profile movements for the clustering model versus annealing time as a function of (a) implant dose and (b) implant energy compared to experimental data from Packan [4].*

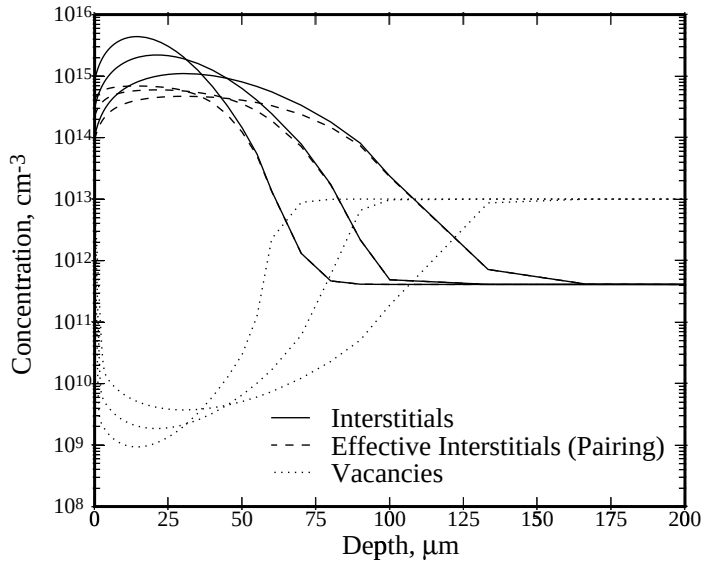

Figure 8: *Interstitial and vacancy profiles as a function of depth for the pairing model after 10, 20 and 40 minutes at 800 for a* $10^{14}\mathrm{cm}^{-2}$ *200 keV implant. Also shown is the effective interstitial profile as limited by the pairing reaction* $(C_\mathrm{I}/(1 + K_\mathrm{AI}C_\mathrm{I}))$.

The resulting logarithmic dependence of transient period on dose agrees with the experimental observations. However, $\Delta R_p \ll D_{\rm I} t$, as clearly seen in Figure 8, so the transient period is independent of energy, in disagreement with experiment. The resulting value of regrowth velocity to provide the best match to the experiments is $\sigma_{\rm I}/D_{\rm I} \sim 10^4 {\rm cm}^{-1}$ at 800°C, which is similar to the value as calculated for very long times from the lateral extent of OED [13]. It should be noted that Park and Law [14] were able to model this same data using a large barrier to Frenkel pair recombination, which contradicts other recent work [10, 15].

For the clustering model, since most interstitials are immobile in clusters, much faster surface recombination is required and the transient period is primarily determined by $D_{\rm I}$. Figure 9 shows a series of simulated defect profiles for the clustering model. Note that the excess interstitial profile extends to substantial depths into the substrate. Again, we can

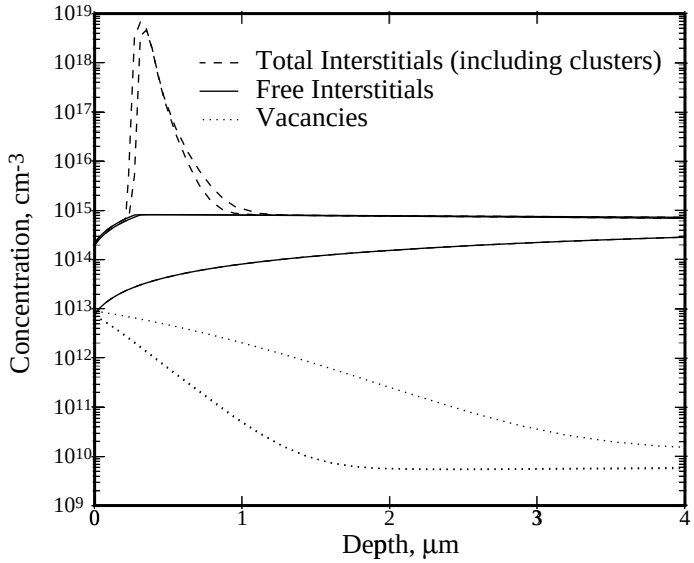

Figure 9: *Interstitial and vacancy profiles as a function of depth for the clustering model after 10, 20 and 40 minutes at 800 for a* $10^{14}{\rm cm}^{-2}$ *200 keV implant.*

estimate the evolution of the net excess interstitial dose

$$\frac{dQ_{\rm I}}{dt} \sim -\frac{D_{\rm I} {C_{\rm I}}^{ss}}{(R_p + D_{\rm I}/\sigma_{\rm I})} \tag{7}$$

The length of the transient period depends on energy through implant range, in agreement with experiments. However, the length of the transient depends nearly linearly on dose, in disagreement with experiment. To match the experimental results, $\sigma_{\rm I}/D_{\rm I} \sim 10^5 {\rm cm}^{-1}$ as calculated for short times [16].

The data for other dopants is much more limited than for boron [5]. No significant arsenic diffusion is observed, presumably because arsenic is such a slowly diffusing species. Phosphorus diffusivity enhancement is about one-fifth that of boron under similar conditions. In the pairing model, peak diffusivity enhancement depends on pairing coefficient for each dopant. In clustering model, peak diffusivity enhancement depends on ${C_{\rm I}}^{ss}/C_{\rm I}^*$, in contrast to experiment. Thus, the differences between boron and phosphorus tend to support the pairing model, but the results are not conclusive due to differences in experimental conditions.

Conclusions

In summary, we have simulated transient enhanced diffusion due to silicon implantation below amorphization threshold. We find that the net defect dose depends on energy and capping layer due to sputtering and knock-ons. A simple analysis shows that the net defect concentrations provide appropriate initial conditions because rapid bimolecular recombination results in very little dopant diffusion while both interstitials and vacancies are supersaturated. We compared an extensive set of experimental data from Packan [4] to simulations and found that neither dopant/defect pairing nor a simple interstitial clustering model alone accounts for the full range of data while remaining consistent with other work. The problem appears to be fundamental to the models in that the pairing model predicts almost no energy dependence, while the clustering model predicts too strong a dose dependence.

Acknowledgements

This work was supported by SRC/SEMATECH grants #91-MC-503 and #93-MJ-530.

References

[1] O. Vancauwenberghe, N. Herbots and O. Hellman, *J. Vac. Sci. Tech.* **B(9)**, 2027 (1991).

[2] J. P. Biersack and W. Ecstein, *Appl. Phys.* **A34**, 73 (1984).

[3] M. D. Giles, *J. Electrochem. Soc.* **138**, 1160 (1991).

[4] P. A. Packan, Ph.D thesis, Stanford Univ., Feb. 1991.

[5] H. Park and M. E. Law, *Appl. Phys. Lett.* **58**, 732 (1991).

[6] N. E. B. Cowern, in **Process Physics and Modeling in Semiconductor Technology**, ed. by G. R. Srinivasan, K. Taniguchi and C. S. Murthy, pp. 20–33 (1993).

[7] W. Taylor, U. Gösele and T. Y. Tan, in **Process Physics and Modeling in Semiconductor Technology**, ed. by G. R. Srinivasan, K. Taniguchi and C. S. Murthy, pp. 3–19 (1993).

[8] U. Gösele and T. Y. Tan, in **Defects in Semiconductors II**, ed. by S. Mahajan and J. W. Corbett, p. 45 (1983).

[9] G. B. Bronner and J. D. Plummer, *J. Appl. Phys.* **61**, 5286 (1987).

[10] S. T. Dunham, in **Process Physics and Modeling in Semiconductor Technology**, ed. by G. R. Srinivasan, K. Taniguchi and C. S. Murthy, pp. 54–65 (1993).

[11] B. J. Mulvaney, W. B. Richardson and T. L. Crandle, *IEEE Trans. Comp.-Aid. Des.* **8**, 336 (1989).

[12] G. J. L Ouwerling, *The PROFILE/PROF2D User's Manual* (Delft University of Technology, 1987).

[13] P. B. Griffin and J. D. Plummer, *Proceedings of the Electrochemical Society Meeting*, San Diego, CA, October 1986.

[14] H. Park and M. E. Law, *J. Appl. Phys.* **72**, 3431 (1992).

[15] E. Guerrero, W. Jüngling, H. Pötzl, U. Gösele, M. Grasserbauer and G. Stingeder, *J. Electrochem. Soc.* **133**, 2181 (1986).

[16] S. W. Crowder, P. B. Griffin and J. D. Plummer, in **Process Physics and Modeling in Semiconductor Technology**, ed. by G. R. Srinivasan, K. Taniguchi and C. S. Murthy, pp. 108–119 (1993).